SUPPLEMENTAL DATA

SUPPLEMENTAL FIGURE LEGENDS

Supplemental Fig. 1. SPRS analysis of PCNA binding by homo- or heteroduplex-bound MutSα. **(A)** SPRS analysis of PCNA binding to heteroduplex-bound MutSα was performed using a streptavidin sensor chip derivatized with 150 RUs of 201-bp heteroduplex or homoduplex DNA. Flow of 200 nM MutSα was initiated at 300 s. At 600 s MutSα flow was either continued (dashed blue line) or supplanted by flow of a solution containing both 200 nM MutSα and 2.5 μM PCNA (red line). RU increase due to PCNA binding was estimated from mean values observed in the presence or absence of PCNA from 650 to 1200 s. Mass bound to homoduplex DNA in the presence of MutSα alone (dashed green line) or MutSα supplemented with PCNA at 600s (orange) is also shown. Mass bound to the heteroduplex substrate upon flow of PCNA alone is depicted by the black line. **(B)** Binding isotherm for PCNA binding to the MutSα•DNA complex as determined from experiments like those shown in **panel A**. Molar stoichiometries were calculated as in **Fig. 1C**.

Supplemental Fig. 2. Experimental and calculated SAXS properties of MutSα and PCNA. **(A)** Experimentally determined scattering profiles (solid lines) (reproduced from **Fig. 4**) are compared with profiles calculated using CRYSOL (1) from crystal structures (dotted) of PCNA (black and grey) (2) and the MutSαΔ341•DNA complex (dark and light brown) (3). **(B)** Forward scattering intensities I(0) (intensity at θ = 0°) for MutSα, MutSαΔ12, MutSαΔ341, PCNA , and a 1:1 mixture of MutSα with the PCNA trimer were determined from concentration-normalized scattering data using the Guinier equation and are plotted versus the molecular weight of each species. **(C)** *Top*, Models shown were generated using the PyMOL program by manually

docking the crystal structures of PCNA (2) and MutSαΔ341 (3) such that the putative complex is in an extended configuration (left and middle) or in a stacked configuration (right), in which the DNA binding channels of MutSαΔ341 and PCNA are aligned so as to permit a linear segment of helix to thread through both. The two extended configurations shown differ in the relative orientation of PCNA and MutSαΔ341 about the y axis (90° relative rotation). *Bottom*, CRYSOL was used to calculate theoretical solution scattering profiles for MutSαΔ341, as well as the extended and stacked model complexes shown in the *Top*. These theoretical profiles were used as input to GNOM (4) to generate P[r] plots shown for MutSαΔ341 (blue line), the two extended (dotted red line and hyphenated green line), or the stacked (dotted blue line) complex.

Supplemental Fig. 3. *Ab initio* shape reconstructions of the MutSα•PCNA complex. **(A)** Two rotational views of seven independent shape reconstructions of the MutSα•PCNA complex are shown (in addition to views depicted in **Fig. 5**). The crystal structures of MutSαΔ341 and PCNA were manually docked into the SAXS envelopes (grey spheres).

Supplemental Fig. 4. R_g dependence on protein concentration. Dependence of apparent R_g on protein concentration is shown for MutSα (blue circles), MutSαΔ12 (green circles), MutSαΔ341 (red circles), MutSαΔ341•DNA complex (brown circles), PCNA (black cirlces), and the MutSα•PCNA complex (orange squares). MutSα, MutSαΔ12 and MutSα•PCNA exhibited a low level of interparticle interaction.

SUPPLEMENTAL REFERENCES

1. Svergun, D., Barberato, C., and Koch, M. H. (1995) *J. Appl. Cryst.* **28**, 768-773

2. Kontopidis, G., Wu, S. Y., Zheleva, D. I., Taylor, P., McInnes, C., Lane, D. P., Fischer, P. M., and Walkinshaw, M. D. (2005) *Proc. Natl. Acad. Sci. U. S. A.* **102**, 1871-1876

3. Warren, J. J., Pohlhaus, T. J., Changela, A., Iyer, R. R., Modrich, P. L., and Beese, L. S. (2007) *Mol. Cell* **26**, 579-592

4. Svergun, D. I. (1992) *J. Appl. Cryst.* **25**, 495-503

Supplemental Fig. 1

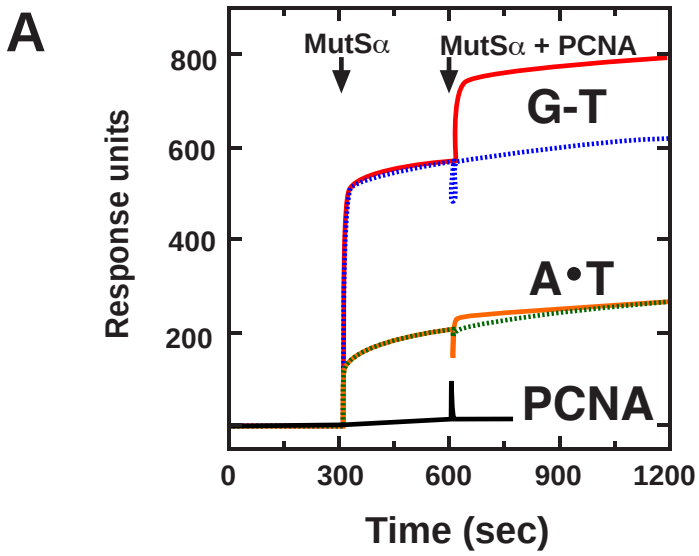

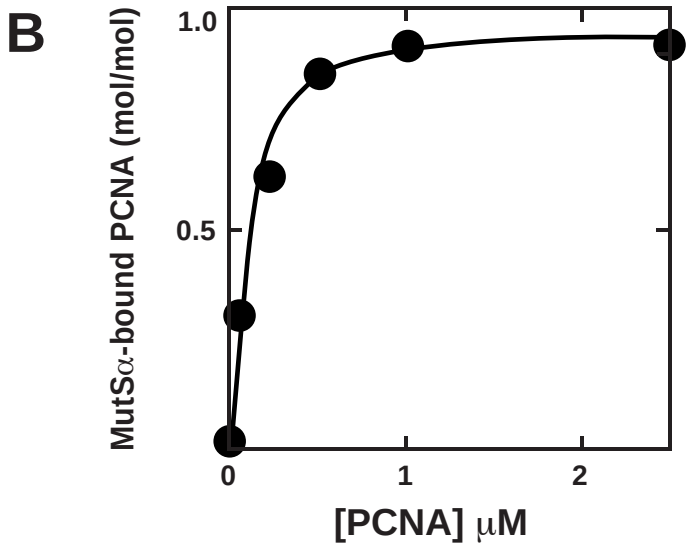

Supplemental Fig. 2

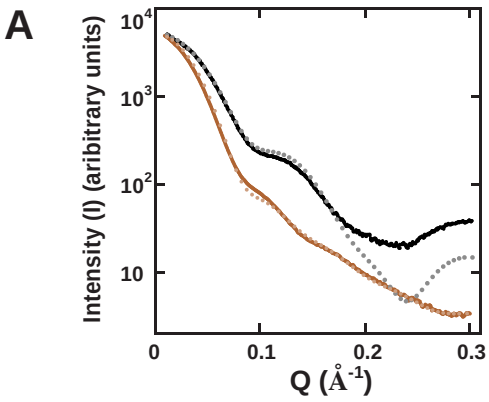

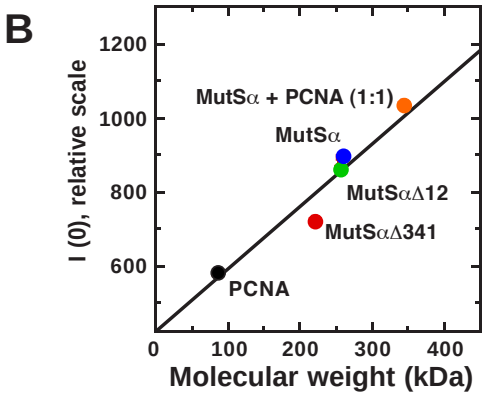

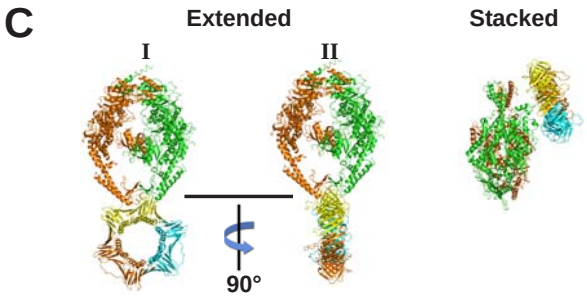

R_g :	59	49
D_{max} :	202	155

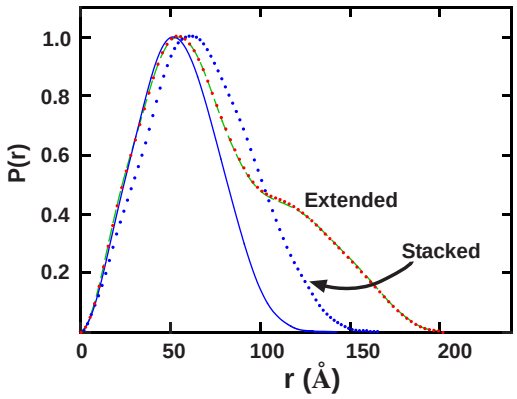

Supplemental Fig. 3

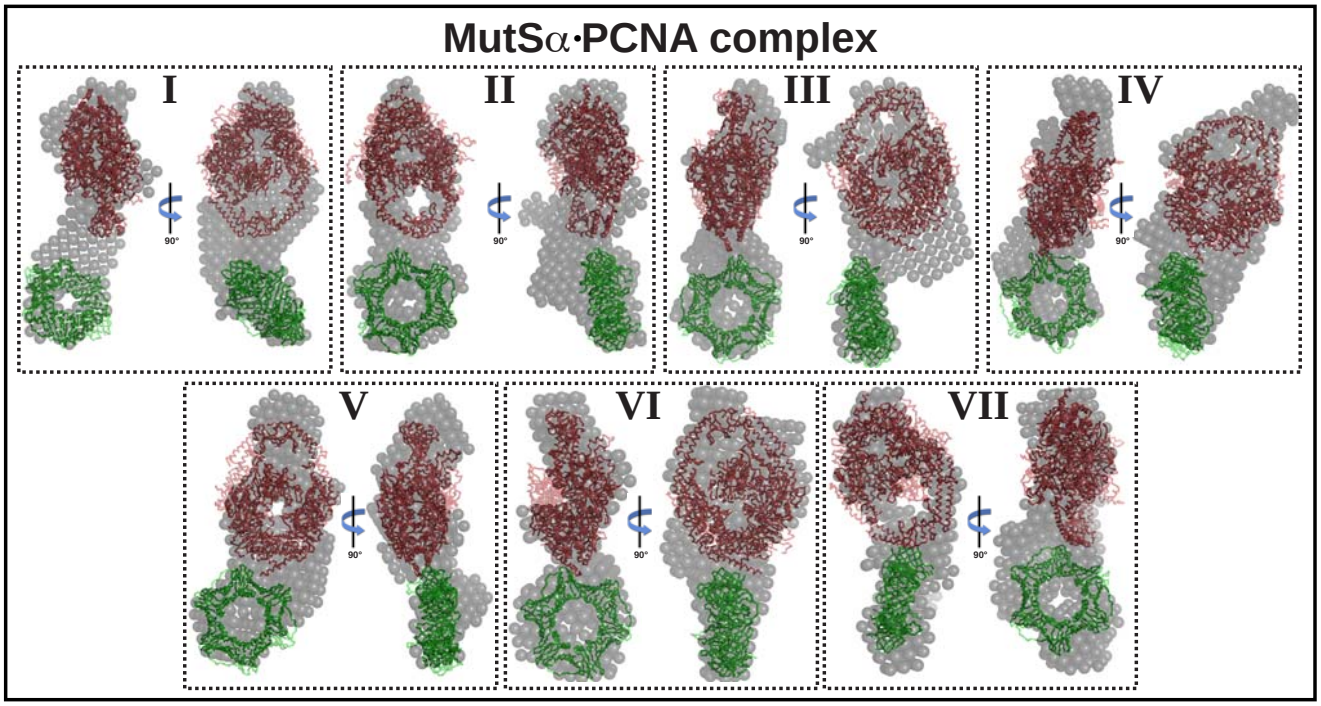

Supplemental Fig. 4